Monthly Notices of the ROYAL ASTRONOMICAL SOCIETY

MNRAS **518,** 1735–1743 (2023)
Advance Access publication 2022 November 11

https://doi.org/10.1093/mnras/stac3063

Computational simulation of the bombardment of molecular clump by realistic cosmic ray field employing GEANT4 code

Maurício T. Pazianotto[1]★ and Sergio Pilling[2]★

[1] *Instituto Tecnológico de Aeronáutica (ITA), São José dos Campos, 12228-900, Brazil*
[2] *Universidade do Vale do Paraíba (UNIVAP), São José dos Campos, 12244-390, Brazil*

Accepted 2022 October 19. Received 2022 October 19; in original form 2022 September 21

ABSTRACT

Here, we present calculations on the energy delivered (and heating) by realistic cosmic rays (CRs) field at a typical molecular clump. The current model describes, with unprecedented spatial resolution, the energy delivery by a realistic CR field in molecular clumps. The calculations were performed employing the Geant4 code (considering full cascade physical processes and hadron physics) considering the cosmic ray field taken from the Voyager spacecraft measurements in the interstellar medium. The results showed that the total energy deposition rate, considering light particles (protons, electrons and alphas), medium-mass ions and heavy-ions, ranges from 400 MeV/g/s in the outer layer (at 10^5 AU) to roughly 100 MeV/g/s in the inner layer of the model (below 0.1 AU). The main energy deposition rate is due to the incoming protons. Incoming alphas represent 15–20 per cent of the energy deposition. In the deep core of the cloud, the fraction of energy delivered by medium-mass ions, electrons, and heavy ions are 5 per cent, 2.5 per cent, and 1 per cent, respectively. The heating induced by cosmic rays seems to affect mostly the regions above ∼500 AU. Considering a balanced heat model with warm dust grains (T∼16–18 K), we observe a small bump in temperature at 2000–5000 AU. We suggest this temperature enhancement by CRs might have some affect on the molecular formation or cometary formation in pristine Oort cloud region inside the Solar System.

Key words: (ISM:) cosmic rays – astroparticle physics – nuclear reactions, nucleosynthesis, abundances – astrochemistry, ISM: clouds, Oort Cloud.

1 INTRODUCTION

Following Williams et al. (2000) molecular clumps (MClumps) are gaseous-rich regions in the interstellar medium (ISM) with typically a parsec size and with typical masses of between 10 and $10^3\ M_\odot$. The average values for density and temperatures of MClumps are around 10^3 H_2/cm^3 and 10 K, respectively (Bodenheimer (2011) and its typical density profile ranges with $r^{-1.5}$ (e.g. Kaufman et al. 1998). Such regions represent one of the initial steps of a star formation (individual or in clusters) (e.g. Bonnell et al. 1997, Seale et al. 2012; Bergin & Tafalla 2007). These clouds are constantly being exposed to incoming energetic particles [e.g cosmic rays (CRs), UV and X-rays] that flow through ISM. The interaction of such energetic particles with matter inside the clouds induce chemical changes as well as gas heating and the study of these phenomena helps to put constraints in the astrochemical models of such objects (e.g. Pazianotto et al. 2021, and references therein). For a detailed review on MClumps and clouds, see also Rigby et al. (2019) and Roman-Duval et al. (2010).

The study of energy delivery by CRs in a typical MC, the precursor evolutionary MClumps, considering full cascade physical processes and hadron physics employing GEANT4 code have been performed recently by Pazianotto et al. 2021 (considering only light ions in the CR inventory), Pilling et al. 2021 (considering both light ions and heavy-mass ions), and Pilling et al. 2022 (considering the most realistic CR flux with light ions, medium-mass, and heavy-mass ions). The authors observed that in MCs the incoming protons are the dominant source in the energy deposition and heating of the cloud, followed by alphas and electrons, with the medium-mass-ion and heavy-ion groups each contributing roughly 8 per cent. Additionally, the model presented by Pilling et al. (2022) shows a temperature enhancement of up to 10 per cent in the external layers of the cloud (reaching 22.5 K) with respect to the previous calculations from Pazianotto et al. (2021), where only light particles were considered. The authors conclude that in the MC model, neither heavy nor medium-mass ions contribute to the temperature enhancement in the deep core of the cloud. The current work aims to apply a similar methodology to determine energy delivery and the heating induced by CRs in a typical molecular clump, a more compact object than the object studied previously. The unprecedented model resolution described here (detailed at distances < 100 AU) helps to put constraints in the physicochemical parameters of star forming regions and might also help to better understand our solar system.

Section 2 presents the computational methodology employed. The main results are given in Section 3 with emphasis on the energy deposition rate and heating by cosmic rays in the different layers within the molecular clump. A comparison with the previous models of MC is also provided. Main conclusions are listed in Section 4.

2 METHODOLOGY

In order to model the geometry and composition of the molecular clump, and also the ionizing particle transport through the object, we have employed the computational toolkit Geant4. v10.5 (Agostinelli

★ E-mail: mtp@ita.br (MTP); sergiopilling@yahoo.com.br (SP)

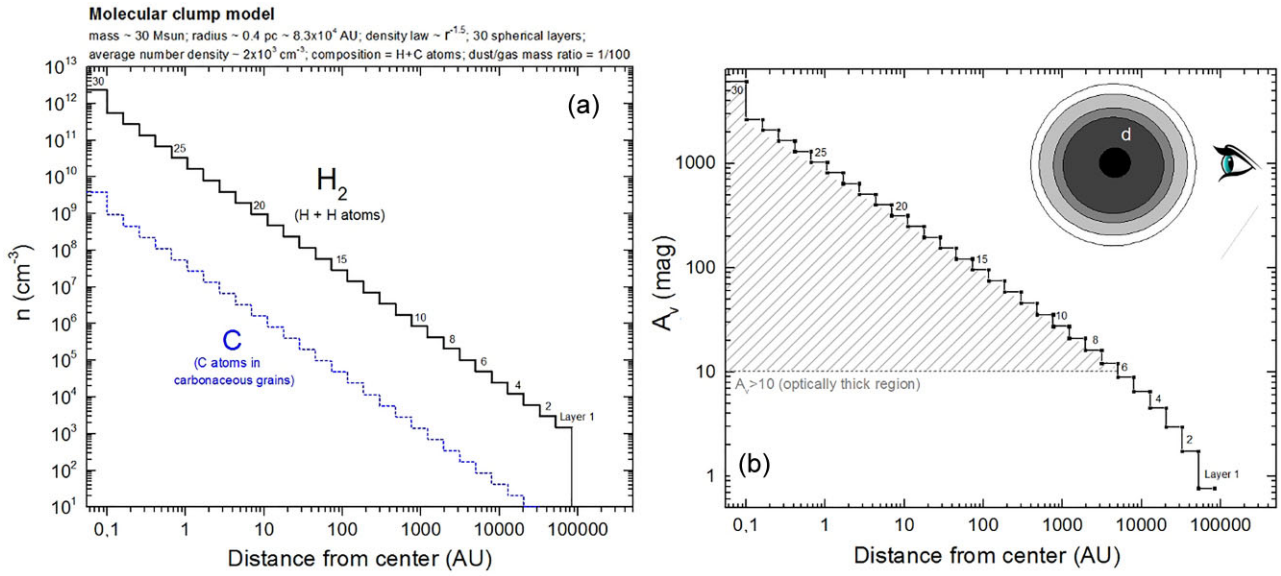

Figure 1. Number density (panel a) and visual extinction profile (panel b) as function of the distance from center of the spherical molecular clump modeled in this work.

et al. 2003; Allison et al. 2006). The geometry considered is a spherical molecular clump with the following parameters in the model: diameter D ∼0.8 pc (∼1.6E5 AU); radius R ∼0.4 pc (∼0.8E5 AU); mass M ∼30 $M_{\odot}$; average particle number density n∼2200 cm^{-3} (mainly constituted by H atoms representing the gaseous H_2 molecules and 1 per cent of C atoms representing the solid fraction of the cloud in terms of interstellar grains) and density law distribution ruled by $r^{-1.5}$; number of concentric spherical layer (with constant number density each), $N = 30$. Fig. 1 presents the number density and visual extinction profile, as function of the distance from center, of the molecular clump modeled in this work. Table A1 (see Appendix) presents the physical parameters (size, mass, density, number density, and average visual extinction) of each spherical layer considered in the model.

In this work, we have taken into account the primary cosmic radiation composed of proton, alpha, carbon, and iron. For all these components, we have used the realistic spectra data from Voyager I Spacecraft measured at the ISM (Cummings, et al. 2016).

The employed cosmic radiation source considers a spherical geometry with radius r ∼0.4 pc (∼0.8E5 AU) that is large enough to cover all the MClump. The source particle is uniformly distributed on the outer sphere represented by blue dots in Fig. 2. We have used the particle emission pointed to inside the volume with different solid angles using the methodology presented by Pazianotto et al. (2021). The simulation of different solid angles emission can provide an estimation of the energy deposition by cosmic radiation in different layers with sufficient statistics. Considering Fig. 2, a simulation was performed varying the theta angle using the following angles: 90º, 30º, 10º, 5º, 1º, 0.1º, and 0.01º. The smaller the emission angle, the better the statistic to estimate the energy deposited in inner layers. Indeed, the solid angle needed should be much bigger than the layer size in order to consider the secondary particle transport properly, as discussed by Pazianotto et al. (2021). The smaller the solid angle emission, the more internal layers can be analyzed. Simulations with smaller theta angles spend more time to be concluded, because the primary particle is focused into regions with higher densities, providing more interactions and computational time.

3 RESULTS AND DISCUSSION

3.1 Energy deposition rate delivered by cosmic rays

Fig. 3 presents the deposited energy rate by the different components of the cascade shower during the collisions of cosmic rays with the simulated molecular clump considering the realistic CR flux. Panels a-c presents the calculation results for the light CR sources (protons, alphas, and electrons), panel d present the calculation results for the iron source, a typical constituent of the heavy-ion group, and panel e present the results for the carbon source, a typical constituent of the medium-mass group. Details about the calculations for the heavy ions group and medium-mass group can be obtained at Pilling et al. (2021) and Pilling et al. (2022), respectively. The relative error was below 5 per cent.

Panel a presents the energy deposition considering the proton source. We can observe an increased energy deposition as a function of distance to the center of MClump for proton and electron particles. For other particle components, one can note an opposite behavior, a higher energy deposition in the center region of the cloud. Moreover, the main particles to energy deposition in all the cloud are proton, electron and positron, respectively. The evolution of energy deposition rate for the cascade particles in the alpha source (panel b) shows that neutrons virtually not contribute to outer layers. For electron source (panel c) energy deposition rate for positrons increases toward the center with for the cascade protons is virtually zero in the center regions. For the iron source (painel d) we observe that in the core region the energy deposition rate for this particle is virtually zero, whereas the cascade electrons are dominant. The energy deposition rates due to cascade muons, pions, and neutrons are virtually negligible at the other layers of the molecular clump cloud. In the deep core, the energy delivered by positrons, deuterons, and tritions are not negligible. The energy deposition rates by photons are virtually constant along the layers of the models.

Fig. 4 presents the total deposited energy rate in the modeled MClump for each primary source considered in this work [e.g. light particles (protons, electrons, and alpha), medium-mass ions

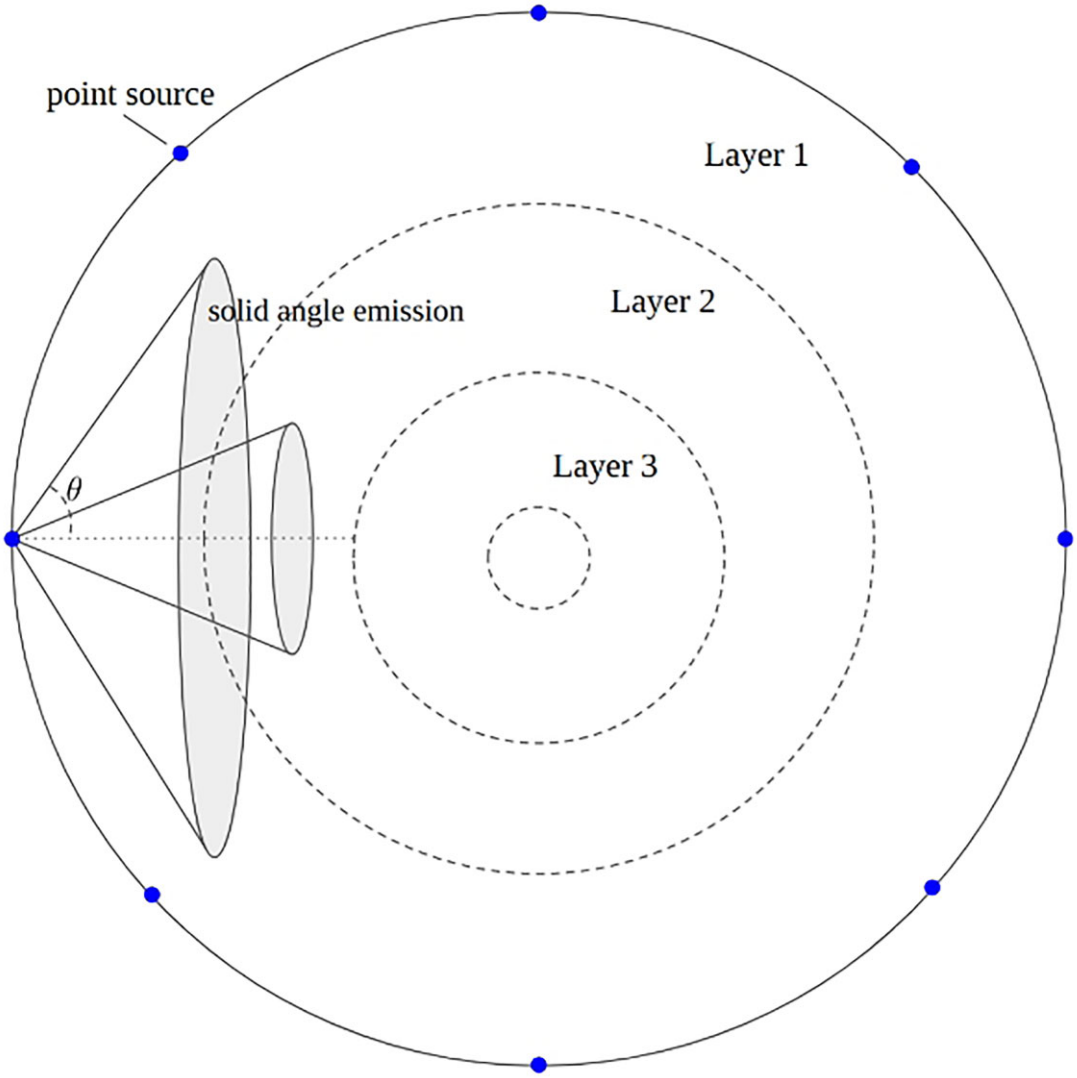

Figure 2. Schematic representation of the source particle distributed on the outer sphere, the solid angle emission and part of the layers considered.

and heavy-ions]. Panels a and b presents the deposited energy rate in units of MeV/g/s and in percentage, respectively, Panel c shows an amplification of panel b for values below 30 per cent. The summed deposited energy (all input of energy from CRs) ranges from 400 MeV/g/s in the outer layer (at 10^5 AU) to roughly 100 MeV/g/s at the inner core (below 0.1 AU).

As observed in previous models (e.g. Pilling et al. 2022) the main energy deposition rate comes from the primary source of protons. In the current work, this corresponds to an energy deposition rate of 250 MeV/g/s at the outer layer and around 80 MeV/g/s in the inner layer of the model (or around 60 per cent of energy input in the outer layers and 75 per cent in the deep core of the cloud). The alpha source represents 15–20 per cent of the energy deposition. In the deep core of the cloud, the fraction of energy delivered by medium-mass ions, electrons, and heavy ions are 5 per cent, 2.5 per cent, and 1 per cent, respectively. In the current model, the maximum energy deposition rate by the heavy ions occurs in the regions between 200 and 300 UA. For alpha particles, the maximum occurs at 0.3 and 0.4 AU. As a summary, protons and the medium-mass ions have the maximum deposition rate at the centre region of the molecular clump. Finally, Fig. 4 also shows that at 1 AU the energy deposition rate of heavy ions is virtually the same as the medium-mass ions, and curiously, from 6×10^2 to 2×10^4 AU, alpha and electron sources present roughly the same energy deposition rate.

For comparison purposes, the normalized deposited energy rate in the modeled MClump for each primary source at 1 AU is shown in Fig. 5. We notice that the largest gradient of energy deposited rate in the models is observed in the case of irons (and as a consequence for the heavy ions group). The second largest gradient of energy deposited rate was observed for electrons.

The stepped features in the plots presented in Figs 3-5 indicated average values in the layers. However, in some positions along the cloud additional features (bumps, valleys, or large steps) are observed in the plots of deposited energy rate, suggesting tentative for explanation: i) A physical effect: in the case of iron bump feature (at $\sim$ 200 AU), it could be explained due to the decrease mean energy of the primary irons as the beam cross the cloud, including the center region; then, part of the iron source with less energy could deposit great part of energy when reach about 200 AU. In the case of the electrons, large steps feature (below 10 AU) a non-linear absorption of electrons in the inner shells might introduce such behavior. In the

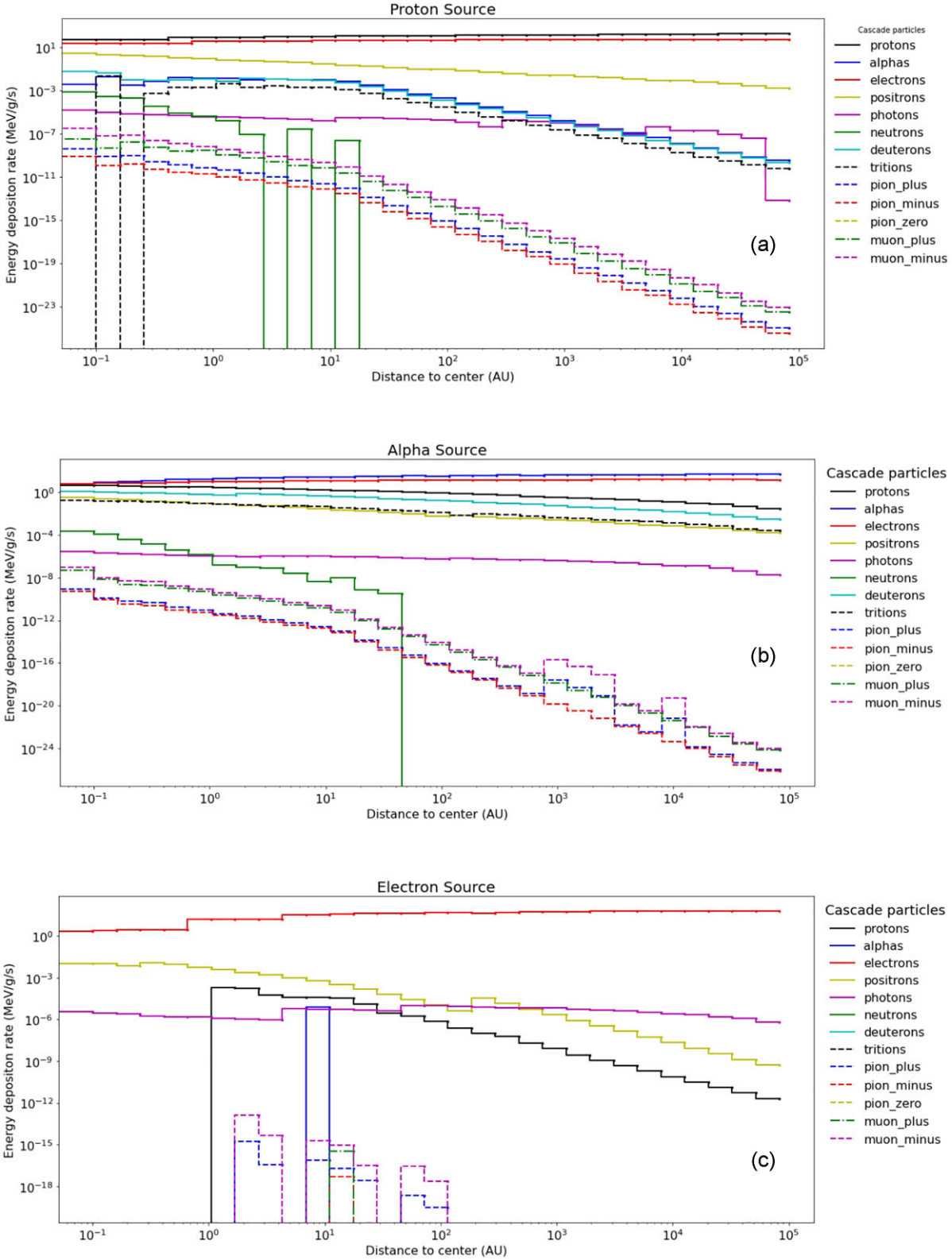

Figure 3. Total deposited energy rate by the different components of the cascade shower during collisions of (a–c) light sources (protons, alphas, and electrons), (d) iron source (a typical constituent of the heavy-ion group), and (e) carbon source (a typical constituent of the medium-mass group) in the simulated MC considering the CR flux data from Voyager spacecraft measured at the ISM. The relative error was below 5 per cent See details in the text.

case of neutrons (see Fig. 3), the observed discontinuity might arise due to its very small half-life (∼10 min) compared with distances toward the cloud. This decay might also introduce some fluctuations in the electrons abundances within the cloud. ii) A numerical effect: the small number of interactions due to low density of the models might introduce such fluctuations in the average values considering the different layers. Future investigations will help to clarify this issue.

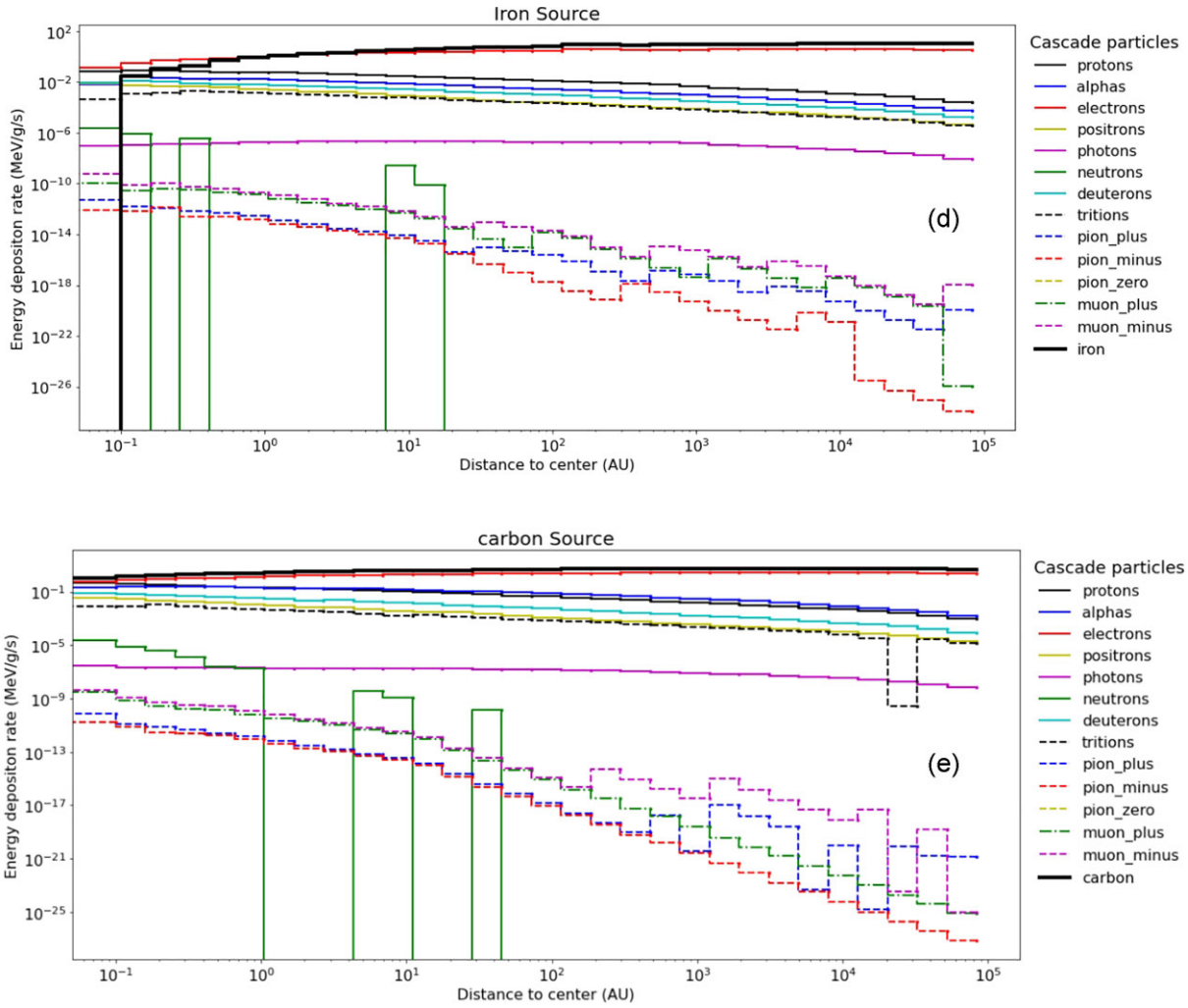

Figure 3. Continued.

3.2 Cloud temperature estimation

It has been suggested that the incoming radiation, mainly the penetrating CRs from the Galactic and extragalactic medium, plays an important role in the heating balance in MCs which has temperatures (from observations) roughly 7–15 K (e.g. Pan & Padoan 2009; Dobbs et al. 2014). In case of MClumps, the typical temperature (excitation temperature) can be little higher, ranging from 5 to 25 K as described by Rigby et al. (2019).

As pointed out by Goldsmith (2001), the temperature profile of MCs should be described by thermal equilibrium condition and respect the balance heat equation in which the incoming energy comes from cosmic rays and stellar radiation and outcome energy is mainly ruled by thermal emission. Pilling et al. (2022), employing the balance heat methodology described by Goldsmith (2001), calculated the typical temperature profile of a MC in the presence of a realistic incoming CR field (containing both light particles, medium-mass ions, and heavy ions). Here we, once more, use this balance heat methodology to describe the heating induced by cosmic rays in a more compact object, a molecular clump with radius around 10^5 AU.

Fig. 6 presents the average gas temperature (or cloud temperature profile) of each layer of the modeled MClump exposed to CRs and considering the balance heat equation described by Goldsmith (2001). Here, we consider different dust temperatures in the calculation, ranging from 6 to 50 K. Panel a shows the *x*-axis in distance from the center of the molecular clump, in units of AU, and panel b the visual extinction (Av) in units of magnitude. For comparison purposes, a ruler with some dimensions inside the solar system is presented at the bottom of the figure. We observe that in all models below around 200 AU the cloud seems not to be heated by the cosmic rays. The model also points out that below 200 AU the gas temperature is very well coupled with dust temperature. All models suggest that outer part of the molecular clumps has temperature around 15 K. For models with dust temperatures below 10 K we observe that cosmic rays can increase gas temperature in the outer parts of the cloud reaching a value around 14 K. Moreover, we observe that for models with dust temperatures ranging from 16 K to 20 K, the cosmic rays, despite not being effective to heat external part of the cloud, produce a slight enhancement (a bump) in the cloud temperature around 3000 AU. In the Solar system this distance lies inside the Oort cloud and might suggest that such CR-induced small heating could have some influence in the cometary formation. This issue should be investigated with detail in future manuscript.

Kalvãns (2016) and (2018) has studied the heating of grains inside interstellar clouds due to collisions with CRs by employing

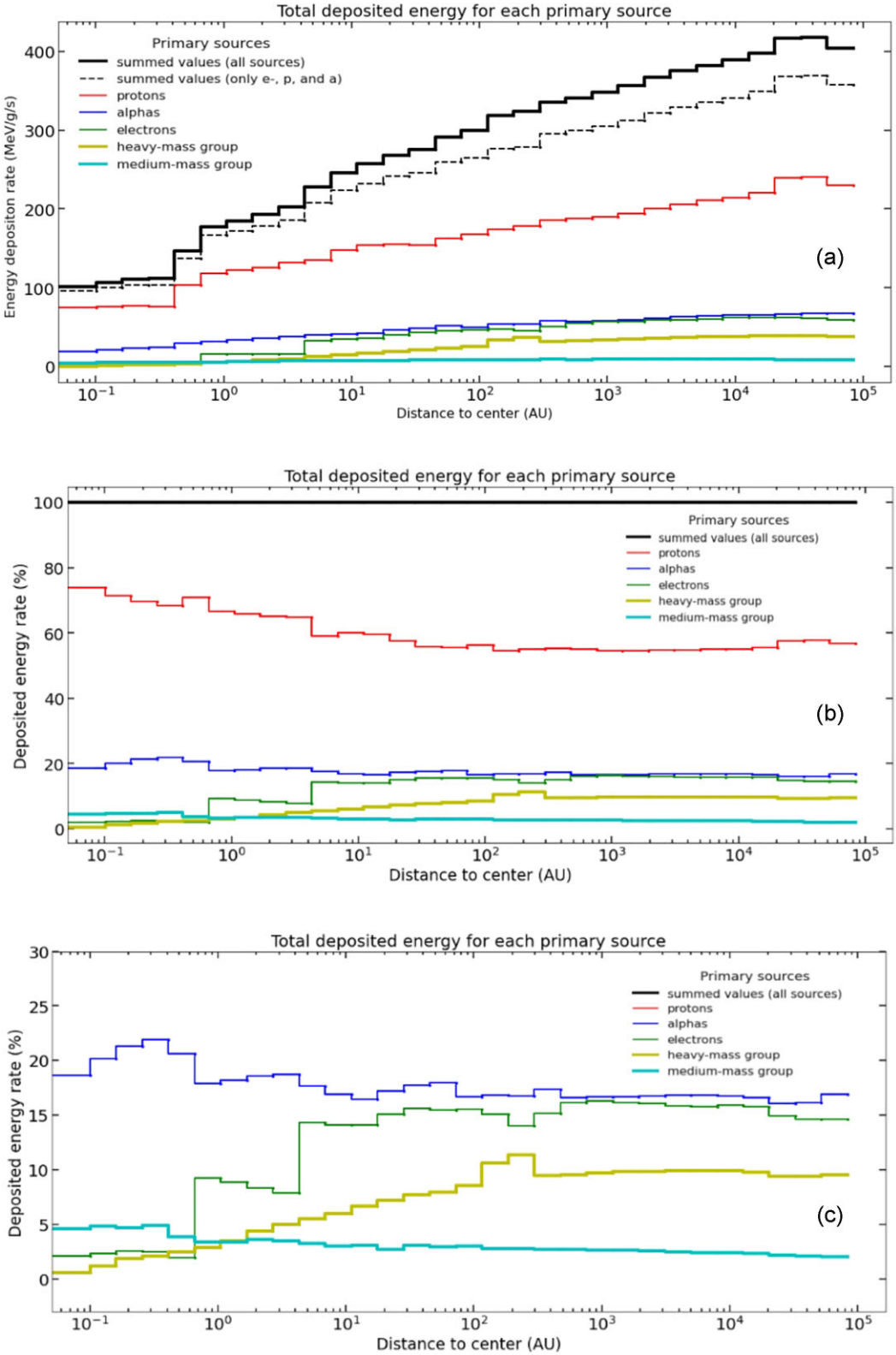

Figure 4. Total deposited energy rate in the modeled MClump for each primary source. Panels a and b present the deposited energy rate in units of MeV/g/s and in percentage, respectively, Panel c shows an amplification of panel b for values below 30 per cent.

a parameterized cosmic ray energy distribution and the energy-loss function from the SRIM code (see Padovani et al. 2009 and Ziegler et al. 2010). The author presented their results in terms of frequency in which grains may achieve a given temperature enhancement during the cloud lifetime and reinforce the importance of CR-induced low-temperature grain heating in interstellar ices. It is worth noting that grain heating by cosmic rays might be characterized by at least two distinct scenarios within the grain: i) the ion track region where local

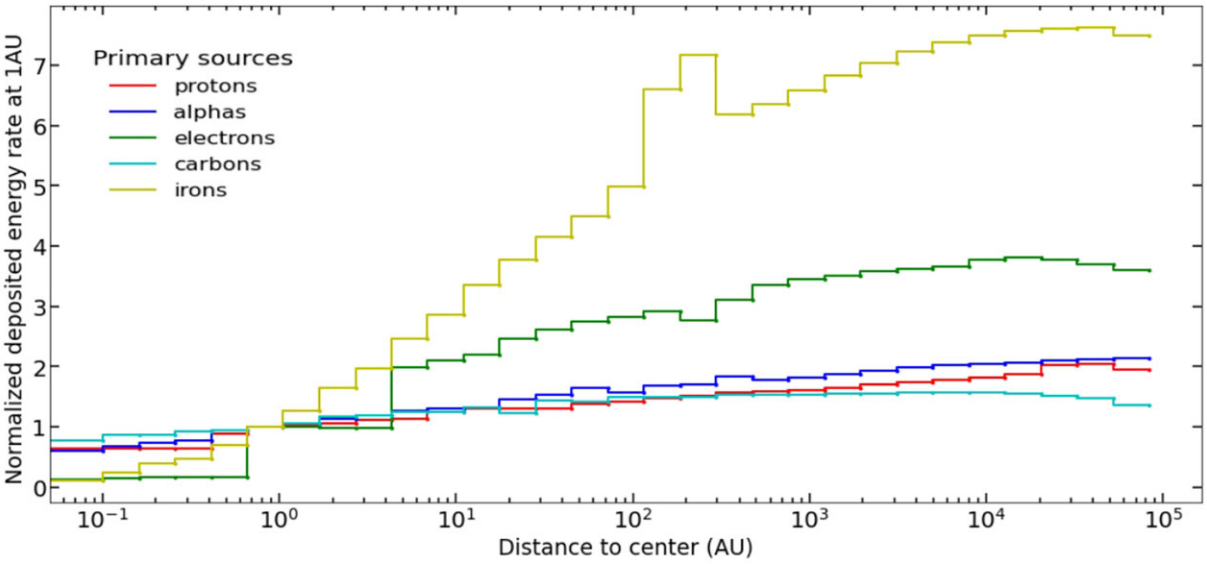

Figure 5. Normalized deposited energy rate in the modeled MClump for each primary source at 1 AU.

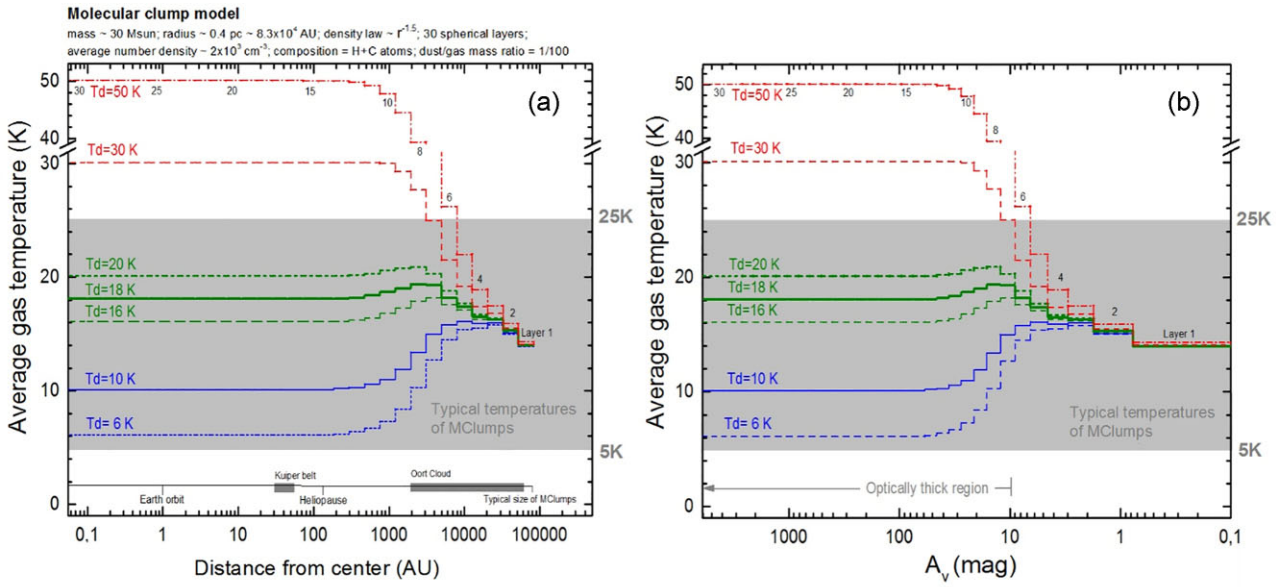

Figure 6. Average gas temperature of each layer of the modeled MClump exposed to CRs and considering the balance heat [Equation (2)]. Each curve was calculated employing different dust temperatures from 6 to 50 K. Panel (a) shows temperature as a function of distance from the center in AU. Panel (b) shows the temperature as a function of the average visual extinction. In both panels, the horizontal gray region indicates the typical temperature range of molecular clumps. The numbers of the layers in the model are indicated by the black labels.

temperature can be extremely high for very short period of time ($\sim 10^{-11}$ s) just after the impact of CR and ii) whole grain region where the temperature might reach hundreds of kelvins due to the heat transfer from the ion track to the entire grain, which happens at larger timescale (10^{-9} s) and is highly dependent of collision frequency and heat capacity of the grain (e.g. Leger et al. 1985; Mainitz et al. 2016). The balance heat considered in the current model indicates that in the obscured part of the cloud the grain temperature is virtually not affected by cosmic rays, which plays a significant role at visual extinction around 2–10 mag (roughly at distances from 2000 to 30 000 AU from the center of the clump).

3.3 Comparison between molecular clump and molecular cloud models

Fig. 7 presents a comparison between the results obtained in current model of energy delivered in the molecular clump cloud (MClump model) and the previous model considering a typical MC model with mass $\sim$ 5400 $M_\odot$, radius $\sim$ 4.8 pc; density law $\sim r^{-1.2}$; 13 spherical layers; average number density $\sim 3 \times 10^2$ cm^{-3}; composition of H + C atoms, and dust/gas mass ratio = 1/100 (Pilling et al. 2022). Panel a presents the total energy deposition rate by cosmic rays on the models, considering both light particles, medium-mass and heavy mass particles (employing realistic cosmic ray flux from

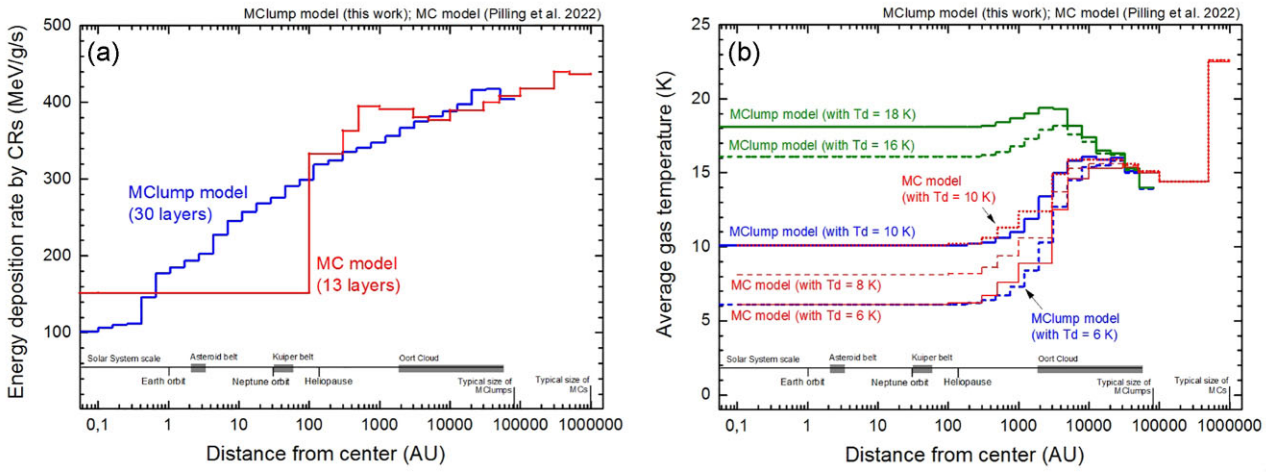

Figure 7. Comparison between the current MClump model and previous MC model (Pilling et al. 2022). Panel a presents the total energy deposition rate by cosmic rays on the modeled objects (considering both light particles, medium-mass and heavy mass particles). Panel b presents the average gas temperature obtained by balance heat equation considering different dust temperatures. Solar system scale is present in the bottom part of the figures for comparison purposes. See details in the text.

Cumming et al. 2016). In this panel we notice that the current model describes, with unprecedented spatial resolution, the energy delivery by a realistic cosmic radiation field in molecular clumps (mainly in the inner part of the cloud). Panel b presents the average gas temperature obtained by balance heat equation (Goldsmith 2001) considering different dust temperatures.

In this figure, we can notice that both models present similarities in energy deposition rates from 10^2 to 10^5 AU. However, the outer part of the MC model (at 10^6 AU) presents a larger energy deposition rate (10 per cent higher) than the outer part of the MClump model (at 10^5 AU). This difference is also expressed in terms of gas heating, indicating that the outer layers of MCs could have temperatures higher than the outer layer of molecular clump (typically 14 K). Curiously, excluding the other layers, in all models considering dust temperatures below 10 K (in both MC model and MC model) we observe a bump in the gas temperature around 2000 AU and 8000 AU. In the case of warmer dust grains (T∼16–18 K) for the MClump model, this bump seems to occur in a slightly small distance to the centre. Comparing these distances with solar System scale, this indicates roughly the distance of Oort cloud comets. Therefore, such small heating induced by cosmic rays in the molecular clouds might have some effect on the chemistry as well as in the gas pressure of matter located in the Oort cloud regions.

4 CONCLUSIONS

In this manuscript, we present the results of theoretical calculations on the energy delivered (and heating) by realistic cosmic radiation fields at molecular clumps. The calculations were performed employing the Geant4 code (considering full cascade physical processes and hadron physics) and the energy distribution of cosmic rays were taken from the Voyager spacecraft measurements in the interstellar medium. The main conclusion were listed below:

i) The total energy deposition rate considering light particles (protons, electrons, and alpha), medium-mass ions and heavy-ions ranges from 400 MeV/g/s in the at outer layer (at 10^5 AU) to roughly 100 MeV/g/s in the inner layer of the model (below 0.1 AU).

ii) The energy deposition rates due to cascade muons, pions, and neutrons are virtually negligible at the other layers of the molecular clump cloud. In the deep core, the energy delivered by positrons, deuterons, and tritions are not negligible. The energy deposition rates by cascade photons are virtually constant along the layers of the models.

iii) The main energy deposition rate comes from the primary source of protons (∼ 60 per cent in the outer layers and 75 per cent in the deep core of the cloud). This corresponds to an energy deposition rate of 250 MeV/g/s at the outer layer and around 100 MeV/g/s in the inner layer of the model. Alpha source represent 15–20 per cent of the energy deposition. In the deep core of the cloud the fraction of energy delivered by medium-mass ions, electrons and heavy ions are, 5 per cent, 2.5 per cent, 1 per cent, respectively.

iv) The largest gradient of the energy deposition rate along the cloud was observed for the iron sources (and consequently the heavy ions). The second-largest gradient was observed for the electron source.

v) Considering the balance heat equation, the heating induced by cosmic rays seems to affect mostly the regions above ∼500 AU. In the case of very low dust temperatures (T ∼ 6 K) the temperature enhancement may reach 15 K (almost three times higher). Considering warm dust grains in the model (T ∼ 16–18 K) we observe a small bump in temperature at 2000–5000 AU (Av ∼ 20–8 Mag) reaching values ∼10 per cent higher. The gas temperature in the outer layers of all molecular clump models is around 14 K.

The current model describes, with unprecedented spatial resolution, the energy delivery by realistic cosmic rays field in molecular clump clouds. We expect the results to put important constraints on the physicochemical parameters and allow a better characterization of such objects in future astrophysical models.

ACKNOWLEDGEMENTS

SP acknowledges the Brazilian research agency CNPq (projects #306145/2015–4; #302985/2018–2). MTP thanks the São Paulo Research Foundation for the financial support (project #2019/13577–0) and LAB-CCAM from ITA for computational support.

DATA AVAILABILITY

The data underlying this article will be shared on reasonable request to the corresponding author.

REFERENCES

Agostinelli S., Allisson J., Amako K. et al. 2003, NIMPA, 506, 250
Allison J., Amako K., Apostolakis J. et al. 2006, ITNS, 53, 270
Bonnell I. A., Bate M. R., Clarke C. J., Pringle J. E. 1997, Mon. Not. R. Astron. Soc., 285, 201
Bodenheimer P.H., 2011, Principles of Star Formation, Astronomy and Astrophysics Library. Springer-Verlag, Berlin Heidelberg
Bergin E. A., Tafalla M., 2007, ARAA, 45, 339
Cummings A.C. et al. 2016, Astrophys. J., 831, 18
Dobbs L. C. et al., 2014, in Bleuther H., Klessen R. S., Dullemond C. P., Henning T., eds, Protostars and Planets VI. Univ. Arizona Press, Tucson, AZ, p. 3
Goldsmith P. F. 2001, Astrophys. J., 557, 736
Kalvans J, 2016, ApJS, 224, 42
Kalvans J, 2018, ApJS, 239, 42
Kaufman M. J., Hollenbach D. J., Tielens A. G. G. M., 1998, ApJ, 497, 276
Leger A., Jura M., Omont A. 1985, A&A, 144, 147
Mainitz M., Anders C., Urbassek H. M. 2016, A&A, 592, A35
Padovani M., Galli D., Glassgold A. E. 2009, A&A, 501, 619
Pan L., Padoan P., 2009, Astrophys. J., 692, 594
Pazianotto M.T., Pilling S., Quesada Molina J.M., Federico C.A., 2021, Astrophys. J., 911, 129
Pilling et al. 2021, Astrophys. J., 921, 116
Pilling et al. 2022, Mon. Not. R. Astron. Soc., 509, 6169
Rigby et al. 2019, AeA, 632, A58
Roman-Duval J., Jackson J. M., Heyer M., Rathborne J., Simon R. 2010. Astrophys. J., 723, 492
Seale J. P., Looney L. W., Wong T., Ott J., Klein U., Pineda J. L. 2012. Astrophys. J., 751, 42
Williams J. P., Blitz L., McKee C. F. 2000, Protostars and Planets IV. Univ. Arizona Press, Tucson, AZ, p. 97
Ziegler J. F., Ziegler M. D., Biersack J. P. 2010, NIMPB, 268, 1818

APPENDIX

Table A1 presents the physical parameters (size, mass, density, number density, and average visual extinction) of each spherical layer considered in the model.

Table A1. Physical parameters of each spherical layer considered in the model.

Layers	External radius (km)	External radius (AU)	Average radius (km)	Mass (Msum)	Mass (g)	Density (g/cm^3)	n_gas (H2/cm^3)	n_dust (C/cm^3)	Av (mag)
1 (outer)	1.24E + 13	8.33E + 04	1.01E + 13	1.52E + 01	3.02E + 34	4.92E-21	1.48E + 03	2.47E + 00	0.77
2	7.78E + 12	5.20E + 04	6.32E + 12	7.49E + 00	1.49E + 34	9.96E-21	3.00E + 03	5.01E + 00	0.97
3	4.86E + 12	3.25E + 04	3.95E + 12	3.70E + 00	7.36E + 33	2.01E-20	6.08E + 03	1.01E + 01	1.23
4	3.04E + 12	2.03E + 04	2.47E + 12	1.83E + 00	3.64E + 33	4.08E-20	1.23E + 04	2.05E + 01	1.56
5	1.90E + 12	1.27E + 04	1.54E + 12	9.04E-01	1.80E + 33	8.25E-20	2.49E + 04	4.15E + 01	1.97
6	1.18E + 12	7.94E + 03	9.65E + 11	4.47E-01	8.88E + 32	1.67E-19	5.04E + 04	8.40E + 01	2.49
7	7.42E + 11	4.96E + 03	6.03E + 11	2.21E-01	4.39E + 32	3.38E-19	1.02E + 05	1.70E + 02	3.15
8	4.64E + 11	3.10E + 03	3.77E + 11	1.09E-01	2.17E + 32	6.84E-19	2.06E + 05	3.44E + 02	3.99
9	2.90E + 11	1.93E + 03	2.35E + 11	5.39E-02	1.07E + 32	1.38E-18	4.18E + 05	6.96E + 02	5.04
10	1.81E + 11	1.21E + 03	1.47E + 11	2.66E-02	5.29E + 31	2.80E-18	8.45E + 05	1.41E + 03	6.38
11	1.13E + 11	7.576E + 02	9.20E + 10	1.32E-02	2.62E + 31	5.67E-18	1,71E + 06	2.85E + 03	8.07
12	7.08E + 10	4.73E + 02	5.75E + 10	6.50E-03	1.29E + 31	1.14E-17	3.46E + 06	5.77E + 03	10.21
13	4.42E + 10	2.95E + 02	3.59E + 10	3.21E-03	6.39E + 30	2.32E-17	7.01E + 06	1.17E + 04	12.91
14	2.76E + 10	1.85E + 02	2.24E + 10	1.59E-03	3.16E + 30	4.70E-17	1.42E + 07	2.36E + 04	16.36
15	1.72E + 10	1.15E + 02	1.40E + 10	7.84E-04	1.56E + 30	9.52E-17	2.87E + 07	4.78E + 04	20.68
16	1.08E + 10	7.22E + 01	8.78E + 09	3.87E-04	7.70E + 29	1.92E-16	5.81E + 07	9.68E + 04	26.16
17	6.75E + 09	4.51E + 01	5.48E + 09	1.91E-04	3.81E + 29	3.899E-16	1.18E + 08	1.96E + 05	33.10
18	4.22E + 09	2.82E + 01	3.43E + 09	9.46E-05	1.88E + 29	7.89E-16	2.38E + 08	3.97E + 05	41.84
19	2.63E + 09	1.76E + 01	2.14E + 09	4.67E-05	9.29E + 28	1.59E-15	4.82E + 08	8.02E + 05	52.98
20	1.64E + 09	1.10E + 01	1.34E + 09	2.31E-05	4.59E + 28	3.23E-15	9.74E + 08	1.62E + 06	66.89
21	1.03E + 09	6.89E + 00	8.37E + 08	1.14E-05	2.27E + 28	6.54E-15	1.97E + 09	3.29E + 06	84.68
22	6.44E + 08	4.30E + 00	5.23E + 08	5.64E-06	1.12E + 28	1.32E-14	3.99E + 09	6.65E + 06	107.1
23	4.02E + 08	2.69E + 00	3.27E + 08	2.78E-06	5.54E + 27	2.68E-14	8.08E + 09	1.35E + 07	135.6
24	2.51E + 08	1.68E + 00	2.04E + 08	1.38E-06	2.74E + 27	5.42E-14	1.64E + 10	2.73E + 07	171.4
25	1.57E + 08	1.05E + 00	1.27E + 08	6.80E-07	1.35E + 27	1.09E-13	3.31E + 10	5.52E + 07	216.7
26	9.83E + 07	6.57E-01	7.98E + 07	3.36E-07	6.68E + 26	2.22E-13	6.70E + 10	1.12E + 08	274.2
27	6.14E + 07	4.10E-01	4.99E + 07	1.66E-07	3.30E + 26	4.49E-13	1.36E + 11	2.26E + 08	347.0
28	3.84E + 07	2.56E-01	3.12E + 07	8.20E-08	1.63E + 26	9.09E-13	2.74E + 11	4.57E + 08	439.1
29	2.40E + 07	1.60E-01	1.95E + 07	4.05E-08	8.06E + 25	1.84E-12	5.55E + 11	9.25E + 08	554;5
30 (inner)	1.50E + 07	1.0E-01	7.50E + 06	5.49E-08	1.09E + 26	7.72E-12	2.33E + 12	3.88E + 09	∼3490

This paper has been typeset from a TEX/LATEX file prepared by the author.